On the Unsteady Shock Wave Interaction with a Backward-Facing Step: Viscous Analysis

N. Mendoza and R.D.W. Bowersox

1 Introduction

Unsteady shock propagation through ducts with varying cross-sectional area occurs in many engineering applications, such as explosions in underground tunnels, blast shelter design, engine exhaust systems, and high-speed propulsion systems. These complex, transient flows are rich in fundamental fluid-dynamic phenomena and are excellent testbeds for improving our understanding of unsteady fluid dynamics.

The shock diffraction over a backward-facing step has been extensively studied via theoretical, computational (CFD), and experimental methods. Previous computational work is overwhelmingly inviscid because it has been well-established that the unsteady Euler equations accurately reproduce the shock propagation, diffraction, and reflections present in these flows (Sun and Takayama [1]). But there have been some discrepancies between experiments and simulations regarding the finer structures, the shear layer, and its instability. As a result, a much smaller number of laminar simulations have been performed to determine if viscosity is responsible for these differences (see Sun and Takayama [1] and Tseng and Yang [2]). These solutions have shown evidence of the Kelvin-Helmholtz instability in the shear layer.

Recent experimental work showed that for the 90° corner, "there is strong evidence of transition to turbulence throughout the flow" (Skews [3]). Indeed, this result indicates a strong need for turbulent simulations. But very few turbulent simulations have been done to date: to the author's best knowledge, only Sun and Takayama [1] and Muritala [4] have modeled the turbulent shock diffraction process over the backward-facing step (BFS). Both studies found that the instability was suppressed by the turbulence model. In addition, a secondary viscous vortex was identified near the corner by Sun and Takayama [1].

N. Mendoza · R.D.W. Bowersox
Department of Aerospace Engineering, Texas A&M University
701 H.R. Bright Bldg., TAMU 3141, College Station, TX, USA

R. Bonazza and D. Ranjan (eds.), *29th International Symposium on Shock Waves 2*,
DOI: 10.1007/978-3-319-16838-8_94

The present work numerically examines the effects of viscosity (laminar) and turbulence (RANS) on the unsteady shock diffraction over the BFS. The effects of the duct height ratio (A_2/A_1) and the incident shock strength (M_S) are also explored. Previous studies have focused on the detailed flow features near the corner, whereas the present study examines the flow fields in much larger physical scales over long periods of time (1-3ms). The numerical results include identifying the effects of viscosity and turbulence on the established wave patterns, quantifying their effects on the primary wave strengths, and discussing their effects on the unsteady shear layer and its instability. These results are directly compared to the theoretical and inviscid results of Mendoza and Bowersox [5], thereby creating a whollistic analysis of the unsteady shock diffraction process over a BFS.

2 Numerical Methods

To obtain these results, the 2D, unsteady Navier-Stokes equations (for the laminar cases) and the 2D, unsteady Reynolds-Averaged Navier-Stokes (RANS) (for the turbulent cases) were solved computationally using the CFD software GASP ^{TM}. The fluid is thermally and calorically perfect air (compressible). The viscosity was modeled by Sutherland's law and the Spalart-Allmaras turbulence model was employed. The simulations are third-order accurate in space (MUSCL, TVD) using the Roe flux scheme with the Harten entropy correction and the modified Essentially Non-Oscillatory limiter around the shocks. The simulations are second-order accurate in time and are implicitly solved using dual-time stepping. The time steps (Δt) and total number of time steps run for each simulation are given in Table 1.

2D structured grids were generated using Pointwise ^{TM}. The domains matched those in Mendoza and Bowersox [5]: the small (entrance) duct was $0.0254m$ high $\times 0.1m$ long, and the large duct was $0.6m$ long. The large duct height was varied to give the desired area ratio: $0.0381m$ for $A_2/A_1 = 1.5$ and $0.0508m$ for $A_2/A_1 = 2.0$. Grid points were clustered towards all walls and the BFS, and total grid sizes are given in Table 1. It was ensured that both laminar and turbulent boundary layers were fully resolved (the wall-integration approach was used), and care was taken to distribute grid points into feature-rich regions. In addition, grid convergence studies were performed. The first $0.05m$ of the small duct was initialized to the post-shock conditions determined by M_S for each simulation, and the remainder of the domain was initialized to freestream conditions ($P_\infty = 101325Pa, T_\infty = 300K, v_\infty = 1e-5m/s$). All walls were set to no-slip, constant-wall temperature boundary conditions, and all flow boundaries were set to first-order extrapolation (non-reflecting).

3 Results and Discussion

First consider the effects of viscosity and turbulence on the established wave patterns. There are six possible wave patterns for the shock interaction with a sudden area enlargement (see Mendoza and Bowersox [5]). For the combinations of M_S and A_2/A_1 considered here, only three of the six are represented (see Table 1). These

Table 1 Simulation Settings

A_2/A_1	M_S	Case	Viscous Mode	$\Delta t(sec)$	Total # Δt	Grid Size
1.5	1.55	3	Lam	5e-7	5,000	919,096
1.5	2.50	5	Lam	3e-7	5,000	919,096
2.0	1.85	6	Lam	4e-7	5,000	1,185,904
2.0	2.50	5	Lam	3e-7	5,000	1,185,904
2.0	1.50	3	Turb	5e-8	50,000	1,465,596
2.0	2.50	5	Turb	5e-8	30,000	1,542,944

wave patterns consist of three primary waves: 1) the transmitted shock (M_{TS}), which is the continuation of the incident shock through the area enlargement (BFS); 2) the secondary shock (M_{SS}), which recompresses the flow expanding from the BFS to the conditions behind M_TS; and 3) the reflected expansion (RE), which accelerates the incoming flow to a sonic velocity at the BFS and acts like converging nozzle.

Instantaneous full-field pressure maps were generated from the solutions. For the both case 3 and 6 simulations, both the transmitted shock and reflected expansion were clearly present. The transmitted shock propagated downstream through the large duct and out of the domain, and the reflected expansion propagated upstream through the small duct and out of the domain. For the case 5 simulations (shown in Figure 1), the reflected expansion was absent, as predicted by the theory, and the transmitted shock was present and propagated downstream. Furthermore, for all viscous simulations, both the transmitted shock and reflected expansion achieved a quasi-steady, quasi-1D state over time, which agrees well with the theory.

However, the primary difference between the theory and the simulations was the shape, structure, speed, and number of the secondary shock, as discussed in Mendoza and Bowersox [5]. The secondary shock was present for all viscous simulations (consistent with the theory), but its shape, speed, and structure were strong functions of time, M_S, and A_2/A_1. The secondary shock also strongly interacted with the boundary layer growing along the duct bottom wall, resulting in a large shock-boundary layer interaction (SBLI). The SBLI changed the secondary shock shape from a "Y"-shaped shock in the inviscid simulations (Mach reflection) to an "X"-shaped shock in the viscous simulations (very large lamdba foot). In summary, the theoretical (inviscid) wave patterns are reproduced in viscous flows as the primary waves each perform a fluid dynamic process that is not detered by viscosity.

The effects of viscosity and turbulence on the primary wave strengths were quantitatively analyzed at very fine time intervals during the simulations. The transmitted shock strength (M_{TS}) and the reflected expansion strength (RE) were computed from time-accurate static pressure data along the duct bottom wall (for details, see Mendoza and Bowersox [5]). The results for M_{TS} and RE are presented in Figure 2, alongside the theoretical and inviscid results from Mendoza and Bowersox [5].

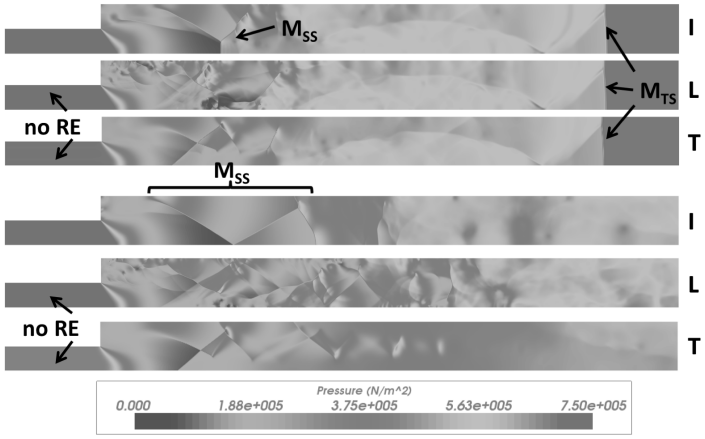

Fig. 1 Pressure Contours, Case 5. (top to bottom) inviscid $t = 7.5e-4sec$, laminar $t = 7.5e-4sec$, turbulent $t = 7.5e-4sec$, inviscid $t = 0.0015sec$, laminar $t = 0.0015sec$, turbulent $t = 0.0015sec$

The viscous results show that viscosity and turbulence decreased M_{TS} from their numerical invscid values by $\sim 0.5-3\%$, which was expected. It is interesting to note that while M_{TS} decreased, it is still higher than its theoretical values. This is most likely due to the net effect of unsteadiness and/or the net compressive effects of the interactions with the secondary flow features (see Mendoza and Bowersox [5]). On the contrary, the viscous results show that viscosity and turbulence actually increased *RE* over its inviscid values (for the case 3 and 6 simulations). Even though viscosity acted to reduce both the high and low pressures involved in the calculation, the pressure *ratio* was decreased, which represents an increase in *RE*.

The effects of viscosity and turbulence on the unsteady shear layer are qualitatively discussed using the instantaneous z-vorticity maps. In the laminar simulations, the shear layer instability was exacerbated (i.e. it shed vortices at a rate higher than in the inviscid simulations), which increased the number of small vortices formed and increased the unsteadiness in the flow field surrounding the BFS. However, in the turbulent simulations, the shear layer instability was damped out over time, which reduced the unsteadiness near the BFS compared to the inviscid simulations. This result is slightly different than those of Sun and Takayama [1] and Muritala [4], who showed that the instability never formed in the turbulent simulations. This difference is due to the shear layer interaction with the reflected shock in the present simulations (which onset the instability), which was absent in [1] and [4].

The secondary shock and the shear layer instability interacted and fought for dominance of the region near the BFS. In the laminar simulations, the lower-pressure small vortices shed by the instability created alternating lower and higher pressure inflow to the secondary shock, which buffeted it and eventually disintegrated it. Each small vortex created a triple point in the secondary shock as they interacted, which shredded the secondary shock into many smaller shocklets.

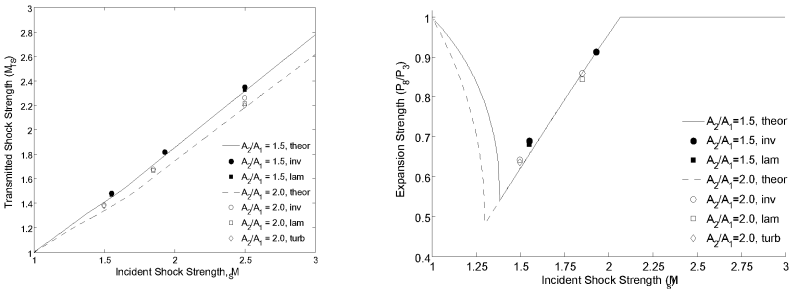

Fig. 2 Effects of Viscosity on Primary Wave Strengths. (left) Transmitted Shock Strength (right) Reflected Expansion Strength

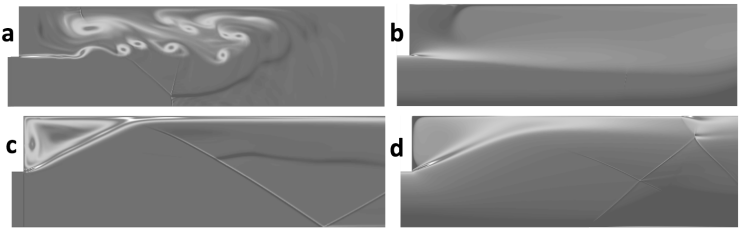

Fig. 3 Long-term Shear Layer Positions. (a) case (1.50, 2.0), inviscid, $t = 1.25ms$; (b) case (1.50, 2.0), turb, $t = 2.5ms$; $(c)case(2.50, 2.0), inviscid$,t=2.5ms; (d) case (2.50), turb, $t = 1.25ms$

In the turbulent simulations, the shear layer instability was largely damped out, which resulted in fewer small vortices being shed, which in turn resulted in a stronger and more stable secondary shock. Thus, in the laminar simulations, the shear layer and its instability dominated the region near the BFS, and in the turbulent simulations, the secondary shock dominated this region. Furthermore, their interaction was affected by A_2/A_1: the larger the area ratio, the more the shear layer dominated; the smaller the area ratio, the more the secondary shock dominated.

The long-term (1-3ms) positions of the inviscid and turbulent shear layers are given in Figure 3, which shows the instantaneous z-vorticity contours at the end of the simulations (case 3 and case 5). After the reflected-shock interaction, the shear layer oscillates but eventually settles in a ”final position” over long periods of time and approaches a quasi-steady state. The shear layer position changes with M_S and over time, but is not affected by viscous mode.

In addition, the first attempt was made to quantitatively measure and calculate the unsteady shear layer thickness. Due to the large spatial gradients in pressure and velocity near the BFS, a new definition for the unsteady shear layer thickness based on vorticity was conceived. This definition was then used to compute the unsteady shear layer thickness for the turbulent simulations at 3-4 downstream locations as functions of both time and distance downstream.

Finally, the secondary viscous vortex was indeed present for the case 3 simulations ($M_S \sim 1.50$), which is consistent with the results of Sun and Takayama [1] and Skews [3]. Furthermore, it did disappear over time, as indicated by Skews [3]. However, the viscous vortex was *not* formed at supersonic values of M_S ($M_S \sim 2.50$) despite the presence of near-wall viscous effects. This interesting result is presently not verifiable due to the lack of published work at $M_S \sim 2.50$.

4 Conclusion

The present study examined the effects of viscosity and turbulence on the unsteady shock diffraction process over a BFS. It was found that the theoretical (inviscid) wave patterns are reproduced in viscous flows. The primary difference between the theory and simulations was the shape, structure, strength, speed, and number of the secondary shock, which was found to depend on time, M_S, A_2/A_1, viscosity, and turbulence. Therefore, it is strongly recommended that further experimental research be conducted to validate the shape and structure of the secondary shock.

Viscosity and turbulence reduced the transmitted shock strength (as expected) by $\sim 0.5 - 3\%$ and increased the reflected expansion strength by $\sim 1 - 2\%$. This small effect is most likely because the primary waves are convective-dominated phenomena and viscosity has not had sufficient time to affect them.

Regarding the unsteady shear layer, it was shown that adding viscosity (laminar) excites the instability (oscillates at a higher frequency than in the inviscid simulations) and adding turbulence damps out the instability (shear layer approaches a quasi-steady state over long periods of time). The shear layer and its instability were shown to interact strongly with the secondary shock. The long-term position and behavior of the shear layer were identified and the first quantitative measurements of the unsteady shear layer thickness are presented (including a new definition of the unstead shear layer thickness). Finally, the secondary viscous vortex was not formed at higher (supersonic) values of M_S.

References

1. Sun, M., Takayama, K.: A Note on Numerical Simulation of Vortical Structures in Shock Diffraction. Shock Waves 13, 25–32 (2003)
2. Tseng, T.-I., Yang, R.-J.: Numerical Simulation of Vorticity Production in Shock Diffraction. AIAA J. 44(5) (2006)
3. Skews, B., Law, C., Muritala, A., Bode, S.: Shear Layer Behavior Resulting from Shock Wave Diffraction. Exp. Fluids 52(2), 417–424 (2011)
4. Muritala, A.O.: Transient Separation of Compressible Flows over Convex Walls. Ph.D. Dissertation, University of the Witwatersrand, Johannesburg, South Africa (2011)
5. Mendoza, N., Bowersox, R.D.W.: On the Unsteady Shock Wave Interaction with a Backward-Facing Step: Inviscid Analysis. In: Proc. 42nd AIAA Fluid Dynamics Conference and Exhibit, New Orleans, LA, USA (2012)